Topographic Analysis of Engagement and Disengagement of Neural Oscillators in Photic Driving: A Combined Electroencephalogram/Magnetoencephalogram Study

Andreas Halbleib, Maciej Gratkowski,* Karin Schwab,† Carolin Ligges,‡ Herbert Witte,† and Jens Haueisen*§‖*

Objective: A coupled system of nonlinear neural oscillators with an individual resonance frequency is assumed to form the neuronal substrate for the photic driving phenomenon. The aim was to investigate the spatiotemporal stability of these oscillators and quantify the spatiotemporal process of engagement and disengagement of the neuronal oscillators in both multitrial and single-trial data.

Methods: White light-emitting diode flicker stimulation was used at 15 frequencies, which were set relative to the individual α frequency of each of the 10 healthy participants. Simultaneously, the electroencephalogram (EEG) and the magnetoencephalogram (MEG) were recorded. Subsequently, spatiotemporal matching pursuit (MP) algorithms were used to analyze the EEG and MEG topographies.

Results: Intraindividually similar topographies were found at stimulation frequencies close to (1) the individual α frequency and (2) half the individual α frequency in the multitrial and the single-trial cases. In both stimulation frequency ranges, the authors observed stable topographies 5 to 10 stimuli after the beginning of the stimulation and lasting three nonexisting periods after the end of the stimulation. This was interpreted as the engaging/disengaging effect of the observed oscillations, because especially the frequency parameter adopted before and after stable topographies were observed. Topographic entrainment was slightly more pronounced in MEG as compared with that in EEG.

Conclusions: The results support the hypothesis of nonlinear information processing in human visual system, which can be described by nonlinear neural oscillators.

Key Words: Electroencephalography, Magnetoencephalography, Photic driving, Matching pursuit, Nonlinear neural oscillators.

(*J Clin Neurophysiol* 2012;29: 33–41)

Brain oscillations, such as the human α activity, are important for human perception and motor control (Başar, 1998). Disturbed oscillations may result in dysfunctional processes. Thus, modulating brain oscillations may be beneficial in both basic research and clinical applications. However, this requires a solid understanding of the neural oscillators. For healthy subjects, it is well known that stimulation by repetitive light flashes yields a frequency locking between the α frequency and the stimulation frequency. Neurons in the human visual cortex synchronize their firing rate to the stimulation frequency of flickering light (Silberstein, 1995). The resulting entrainment of the α activity in the EEG appears in changes of the α frequency toward the stimulation frequency (Gebber et al., 1999; Herrmann, 2001; Rager and Singer, 1998). Clinically, this effect is called photic driving and serves as an indicator of the functional flexibility of the cortex and as an activation method in clinical practice, for example, in epilepsy, schizophrenia, or other neuropsychiatric diseases (Jin et al., 1997; Lazarev et al., 2006; Takahashi et al., 1998).

A fundamental examination of the photic driving effect in the human EEG was given by Herrmann by stimulating from 1 to 100 Hz in 1-Hz steps (Herrmann, 2001). Miranda de Sa and Infantosi (2005) showed that stimulations close to the α peak were most effective. Photic driving in the EEG and the MEG was first quantified by Kalitzin et al. (2002) and Parra et al. (2003).

Topographic effects of encephalographic photic driving effects in the case of children and adolescents were described by Lazarev et al. (2004), for patients with migraine by de Tommaso et al. (2003), and for patients with schizophrenia by Jin et al. (1998).

Schwab et al. (2006) performed for the first time a photic driving experiment that simultaneously recorded EEG and MEG with a high density of stimulation frequencies, which were adapted to the individual α rhythm of each volunteer. They showed that the α peak in the power spectra is significantly elevated when stimulating at or close to the individual α frequency of the volunteer ($\sim$0.9–1.1α). A fixed response frequency (plateau) in the EEG and MEG recordings was obtained for all stimulation frequencies close to the individual α frequency. A similar response could be shown for stimulation frequencies around half the individual α ($\sim$0.45–0.55α). These findings supported the hypothesis that the functional basis for this phenomenon is formed by a coupled system of nonlinear neural oscillators with an individual resonance frequency. A pure linear system would respond with high mean amplitudes around the resonance frequency. The fixed resonance plateau matching the individual α frequency indicates nonlinear behavior. Additionally, the presence of harmonic and subharmonic resonance peaks leads to the conclusion that the involved oscillators exhibit a nonlinearly coupled system. This interpretation contributes to the findings of Stam et al. (1999) suggesting that the human α rhythm behaves in a nonlinear fashion.

Based on this hypothesis, the aim of this article was (1) to perform a topographic analysis of the spatial patterns in MEG and EEG multichannel recordings to investigate the spatial stability of the assumed underlying neuronal oscillators. Our hypothesis is that intraindividually similar EEG and MEG topographies during the plateau phase exist. Second, we (2) aimed to quantify the spatiotemporal process of engagement and disengagement of the neuronal oscillators in both the multitrial and single-trial data by investigation

From the *Institute of Biomedical Engineering and Informatics, Ilmenau University of Technology, Ilmenau, Germany; †Institute of Medical Statistics, Computer Sciences and Documentation; ‡Departments of Child and Adolescent Psychiatry; §Neurology, Biomagnetic Center, Friedrich Schiller University Jena, Jena, Germany; and ‖Department of Applied Medical Sciences, King Saud University, Riyadh, Saudi Arabia.

Address correspondence and reprint requests to Jens Haueisen, Prof. Dr. -Ing. habil., Institute of Biomedical Engineering and Informatics, Ilmenau University of Technology, PO Box 100565, D-98684 Ilmenau, Germany; e-mail: Jens.Haueisen@tu-ilmenau.de.

ISSN: 0736-0258/12/2901-0033

of transient behavior of the spatial topographies. Therefore, we analyzed the same photic driving data that were considered in Schwab et al. (2006) with the help of spatiotemporal MP algorithms.

MATERIALS AND METHODS

Matching Pursuit

The basic approach of the iterative MP algorithm is to iteratively decompose a real time series, for example, the EEG, into an approximation $f(t)$ of a sum of weighted Gabor atoms.

$$f(t) = \sum a_n \times g_{\gamma_n}(t), \quad (1)$$

where a_n represents the weights and $g_{\gamma_n}(t)$ are atoms.

The waveforms or so-called (Gabor) atoms are constructed from a (Gaussian) window function, which is modulated by a sinusoidal function of a fixed frequency and includes a phase shift ϕ_{MP}. Consequently, an atom is well localized in time t and frequency f; as an additional parameter, the window function can be scaled.

$$g_{(\gamma,\varphi)}(t) = \frac{K_{(\gamma,\varphi)}}{\sqrt{s}} \times g\left(\frac{t-u}{s}\right) \times \cos\left(\xi t + \phi_{MP}\right), \quad (2)$$

where s is the scale, u stands for translation, and ξ represents modulation; $\gamma = (s,u,\xi)$; $K_{(\gamma,\phi)}$ is a normalization factor so that $|g_{\gamma,\phi}(t)| = 1$ Please note that, in contrast to wavelet analysis, the parameters are independent.

The MP method allows for a concise signal approximation by a small number of atoms. The algorithm chooses the atoms from a set, the dictionary. In theory, the dictionary can be composed of an infinite number of atoms. In praxis, their number in the dictionary is limited, but a large amount of atoms, and with it high redundancy, are preserved. Thus, MP has a large amount of possible waveforms for describing features in a signal but uses only a few in the final approximation. This is a contrast to Fourier analysis, which works on an orthogonal base and thus needs many sinusoidal functions to approximate a signal.

A signal approximation by MP atoms is calculated iteratively. In the first step, the algorithm correlates a given single channel data set with each atom in the dictionary. The atom with the highest correlation—and therefore the highest inner product with the signal—serves as the first approximation of the signal. Subtracting the first atom from the signal yields the first residual. The algorithm repeats these two steps producing the second atom and second residual. This recurs until a criterion, such as a predefined number of atoms or a predefined percentage of explained energy, is met. After m iterations, the signal can be written as the linear combination of m atoms plus a residual (Mallat and Zhang, 1993). We call the set of m atoms an atom set. In an atom set, the atoms are ranked by the fraction of the energy they account for. The first approximation on a signal is therefore the first atom in an atom set.

The value of inner product depends on the parameter combination. If the MP algorithm approximates a signal, the parameters will be chosen so that the best overlay is produced. This applies besides to, for example, frequency parameter also to the translation parameter. Thus, the algorithm also determines the best time index for each atom in the observed timeframe.

For the analysis of the multichannel EEG and MEG recordings, we applied an extension of the MP algorithm, which is suitable for multichannel analysis: the topographic matching pursuit (TMP) algorithm (Gratkowski et al., 2007, 2008). The TMP uses a standard MP dictionary of Gabor atoms. The key difference between TMP and standard MP lies in the correlation: The TMP algorithm chooses the atom that has the highest simultaneous correlation in all channels. Hence, the channels are approximated by identical parameters except for different amplitudes and phases for each channel. Topographies approximated by TMP vary over time. An extensive description of TMP and other spatiotemporal MP techniques can be found in Gratkowski et al. (2007, 2008).

Data/Experiment

The responses of 10 volunteers (mean age 28.8 ± 5.81 years, 5 male; 5 female) to flicker stimulation were recorded simultaneously with MEG and EEG. The stimuli were delivered via optical fibers from 2 light-emitting diodes, 9 cm away from the closed eyes of the subjects. The 32-channel EEG (Synamp, Compumedics Neuroscan, El Paso, TX, USA) was recorded with 10-20 system over the frontal region and with a 10-10 system over the occipital region. Additionally, an MEG with 31 channels (Philips, Hamburg, Germany) was recorded over the occipital region (Fig. 1). Both EEG and MEG were recorded at a sampling rate of 1 kHz and a hardware bandpass filter between 0.1 and 300 Hz.

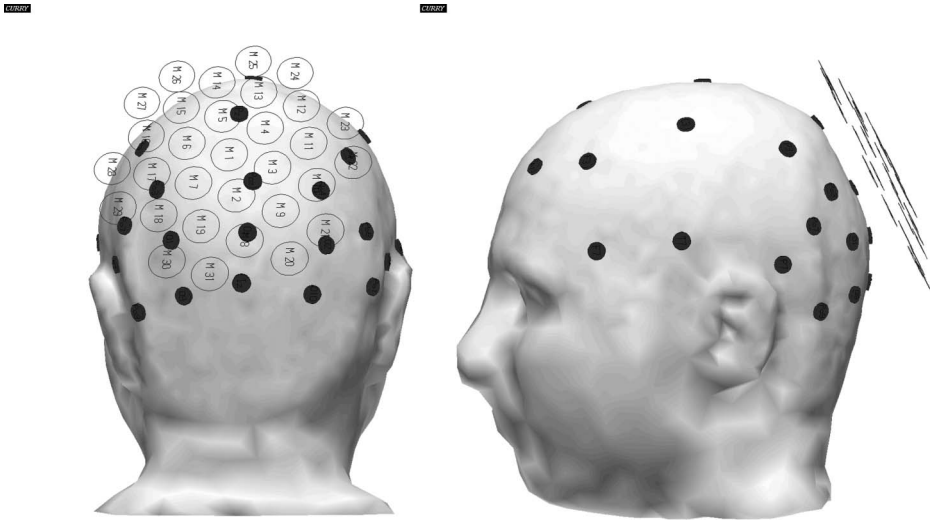

FIG. 1. Positions of the electroencephalogram (EEG) electrodes (black disks) and the magnetoencephalogram (MEG) pick-up coils (black circles) during the simultaneously recorded EEG and MEG: **A,** back view and **B,** side view.

Before the actual experiment, the individual resting α frequency was measured. It ranged from 9.5 to 11.8 Hz (Schwab et al., 2006). Next, the volunteers were stimulated with light flashes of frequencies with a fixed ratio to the individual α frequency ranging from 0.4 to 1.6 times the individual α frequency (Fig. 3). The frequency steps around 0.5α and 1α were narrower. An overview of the experimental design of the study is given in Figure 2.

Because of the variety of individual resting α frequencies, the various stimulation periods for all the subjects and frequencies were different. For example, the stimulation period for 0.4α had a range from 212 to 264 milliseconds and the stimulation period for 1.6α from 52 to 66 milliseconds. These periods are valid for multitrial and single-trial analyses. Therefore, time points relative to the beginning of a stimulation period as a reference point could not be expressed in milliseconds but as multiple (<1) of the individual stimulation period $T_{i,\mathrm{fr}}$.(i is the individual; fr is the stimulation frequency).

The following stimulation frequencies were presented: 0.4, 0.45, 0.5, 0.55, 0.6, 0.7, 0.8, 0.9, 0.95, 1, 1.05, 1.1, 1.2, 1.4, and 1.6 times the individual α frequency. Thus, all the frequencies were expressed as multiples of the individual α frequency. Each stimulation frequency was presented in a block of 20 trains. A resting period of 30–60 seconds existed between the stimulation blocks of different stimulation frequencies. Each train consisted of 40 flicker periods (50% on and 50% off cycles for each frequency). Between 2 trains, there was a resting period of 4 seconds (Fig. 2). For preprocessing, we filtered the data with a zero phase Butter worth bandpass filter of order 4 between 2 and 20 Hz. The stimulation blocks were processed separately as described in the next sections.

Reference Atoms

We first examined the stimulation frequency at the individual α frequency of each volunteer. It consistently produced the highest signal-to-noise ratio and presumably the most stable topography. We averaged data over 20 trains so that only 1 train, representing 1α, remained per volunteer. For each of the 40 stimuli in that train, we calculated the corresponding 40 TMP atom sets with a length of 125 milliseconds and with an iteration depth of $m = 10$ atoms. Additionally, we computed in a similar fashion the atom sets at the virtually after 10 stimulations after the end of the 40 real stimulations. This

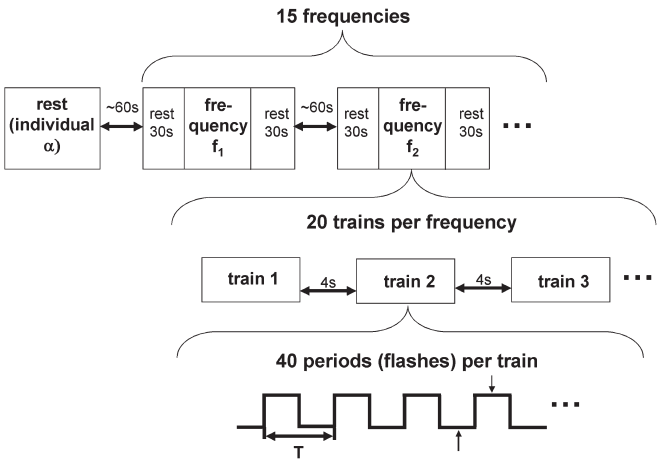

FIG. 2. Experimental design of the study. The light-emitting diodes were on for 0.5 T for each frequency. The increase and decay time for the light-emitting diodes were measured to be 100 microseconds.

was done, because it is assumed that the frequency entrainment will last after the end of the real stimulation.

For all except the virtual atom sets, we performed a paired t-test. We compared the energy content of an atom set with the energy content of each atom of the same set. We found that only the first atoms (atoms of the first iteration, $m = 1$) of each atom set were significant at a 5% significance level of the t-test. Therefore, further analysis was conducted with the first atoms only. From these 40 atoms ($m = 1$) calculated at 1α, we computed the average atom for each volunteer separately for the EEG and the MEG. This average atom is called reference atom in the following. For each volunteer, an individual reference atom is used. The topography of a reference atom varies over time, because there is a phase shift between the channels.

To quantify the similarity of the observed topographies, we calculated the correlation coefficients (ccs) between the reference atom and the 40 atoms used for building the reference atom, including the 10 virtual stimulation atoms after the end of the real stimulation. For each of the 40 + 10 stimulation periods, we obtained 1 cc per channel. Expressed in a different manner, we obtained 1 sequence of 40 + 10 ccs for each channel reflecting the 40 + 10 stimulation periods.

For each sequence, we calculated the mean and the SD of the first 40 ccs. The SD was applied as a statistical measure to categorize the 40 + 10 ccs: Inside the 90% confidence interval, they were accepted (Eq. 3).

$$\mathrm{cc} > \mathrm{mean}(CSeq) - \frac{1.645 \times \sqrt{\mathrm{Var}(CSeq)}}{\sqrt{k}}. \qquad (3)$$

$Cseq$ denotes a correlation sequence of $k = 40$ ccs. $\sqrt{\mathrm{Var}(CSeq)}$, is the SD of the correlation sequence.

In the next step, the reference atom obtained for each volunteer at the stimulation frequency of 1α is used for the similarity analysis of topographies at the other stimulation frequencies.

Similarity of Topographies Between Different Frequencies

The filtered data were averaged over the 20 trains of each stimulation frequency so that only 1 train per frequency and per volunteer remained. For the averaged train of each stimulation frequency, we calculated TMP atoms with an iteration depth of $m = 10$. Atoms of length 125 milliseconds were computed. The atoms were calculated so that the absolute maximum of the global field power (GFP) of a stimulation period was included. The maximum for each volunteer occurred relative to the onset of a stimulation period at approximately $0.9T_{i,\mathrm{fr}}$. The time point of this maximum was determined across stimulation frequencies and volunteers. Thus, the stimulation onset, individual length of the stimulation period, and the time point of the maxima determined the timeframe (with a length of 125 milliseconds) in which the atoms were calculated. The exact time index (translation) of the atoms was determined by the algorithm through an optimization of the translation parameter u. Even for not well phase locked cases, optimization of the translation parameter u ensures the approximation quality. Please note that for each of the 10 volunteers and each of the 15 stimulation frequency atoms had to be calculated for 40 + 10 stimulations (see Section 2.3) accumulating to 7,500 atoms.

Over all 10 volunteers, 15 stimulation frequencies, and 40 (real) stimulation periods, thus 6,000 atom sets (with 10 atoms each), we performed paired t-tests of the energy distribution of an atom set

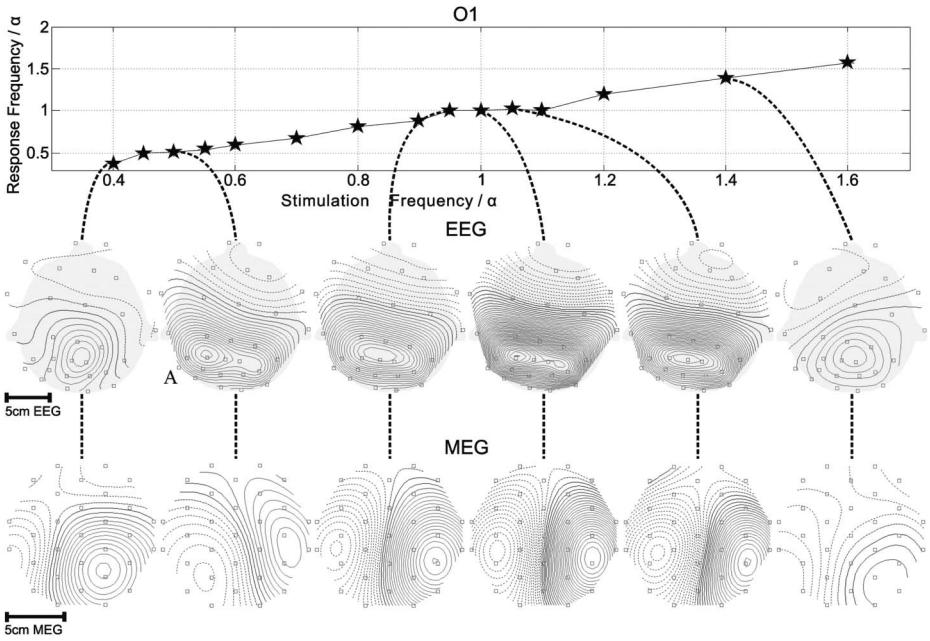

FIG. 3. Top: Frequency entrainment for one volunteer. Ratio of flicker stimulation frequency to α at rest on the abscissa is plotted against the response frequency to α at rest on the ordinate (electroencephalogram [EEG] channel O1). The star indicates the obtained response frequency for a given stimulation frequency (normalized to the individual α frequency). A frequency plateau around 0.5 and 1α can be observed. Middle and bottom: Corresponding EEG and magnetoencephalogram topographies at stimulation frequencies 0.4α, 0.5α, 0.95α, 1.0α, 1.05α, 1.4α. The topographies observed for 0.5α and around 1α are similar. The line increment is identical in all figures: 0.5 μV and 10 fT per line, respectively.

versus energy content of each atom in the atom set. We found that all atoms from the first iteration ($m = 1$), only 5 atoms from the second iteration ($m = 2$), and no atoms from all further iterations contributed significantly to the energy of the set of atoms at a 5% significance level of the *t*-test. Consequently, in the subsequent correlation analysis, we used only the first atom (i.e., the one obtained in the first iteration) of each set of atoms.

As indicated in the previous section, the averaged atom (reference atom) calculated at 1α served as reference for the correlation analysis. For each volunteer and stimulation frequency, we calculated (channelwise) correlation sequences between the reference atom and each of the 40 + 10 first atoms. From each of the 40 + 10 correlation sequences, we selected the ccs obtained at the index with the highest simultaneous correlation in all channels. The selected ccs quantify the (channelwise) similarity between the reference atom and the atom under consideration. For 1 stimulation period (of 1 volunteer and stimulation frequency), this yielded a vector of 32 ccs for the EEG case and a vector of 31 ccs for the MEG case. Next, we concatenate the vectors from all stimulation periods (of one volunteer and stimulation frequency) according to the type of recording. This yielded for each volunteer and stimulation frequency a series of 40 + 10 ccs for each of the 32 EEG channels and 31 MEG channels. We name this series of ccs a cc sequence (note: do not misinterpret this as correlation sequence). A total of 300 cc sequences were calculated for the 10 volunteers and 15 stimulation frequencies and recording modalities (EEG/MEG).

For categorization of the results, we proceeded as follows. Weak channels of crosscorrelation sequences were discarded. A channel was considered weak if its mean was outside the 90% confidence interval of the mean of a crosscorrelation sequence (Eq. 3). Furthermore, and similar to Section 2.3, we calculated for each channel of these sequences the mean and the SD of the first 40 coefficients. Analogous to Section 2.3, ccs inside the 90% confidence interval were accepted.

Single-Trial Analysis

In contrast to the earlier steps, the atoms were now computed for the single-trial data. Thus, no averaging across the recorded trains took place. Instead, the correlation sequences were averaged. This prevents an eventual smoothing out of responses that are not well phase locked to the stimulus, which may occur at stimulation frequencies outside stimulation frequency plateaus. Single-trial analysis implied calculating TMP atoms for each of the 40 + 10 stimulations of 20 trains for each of the 15 stimulation frequencies per volunteer for EEG and MEG (300,000 atoms). We used the same reference atoms described in Section 2.3. As before, only the first atom of each atom set was used.

Thus, for each volunteer, correlation sequences were calculated between 2,000 (20 trains at 40 + 10 stimuli per EEG and MEG) single-trial atoms per stimulation frequency and the respective MEG or EEG reference atom.

We correlated the crosscorrelation sequences and the autocorrelation sequence of the reference atom. The ccs obtained at 100% overlap of the 2 correlation sequences (zero lag) represented the similarity of all approximated channels of 1 stimulus to the reference. From the ccs of the stimuli of 1 stimulation frequency and 1 trial, we produced cc sequences. Next, we averaged over the 20 cc sequences of one stimulation frequency, so that we obtained a sequence of 40 + 10 ccs per stimulation frequency.

RESULTS

Frequency Entrainment Topographies

Figure 3 shows the typical frequency locking as reported in Schwab et al. (2006). Similar topographies can be observed around 0.5α and around 1α for both EEG and MEG. The topographies as depicted in Figure 3 developed at fix latencies relative to each stimulus onset and coincided with the maxima in the GFP. This latency was $0.9T_{i,\mathrm{fr}}$ (with $T_{i,\mathrm{fr}}$ being the individual period duration [Section 2.3]). These topographies appeared only in the plateaus around 0.5α and 1α, outside of the plateaus the topographies were not observed. The strong positive EEG activity can be found in occipital regions with a maximum around Po3, Poz, and Po4 extending to P3, Pz, P4, O1, Oz, and O2.

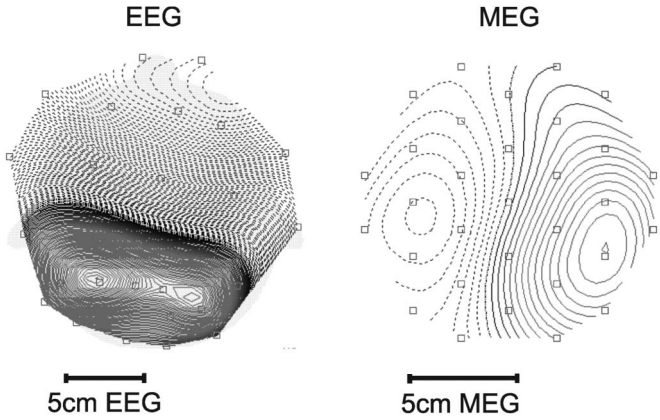

FIG. 4. Mapping of the reference atom at maximum global field power of one volunteer (same volunteer as in Fig. 1). The central frequency of this atom is 10.63 Hz. The measured individual resting α frequency for this volunteer was 10.64 Hz.

Next, we analyzed the similarity of the spatiotemporal topographies for the stimulation frequency 1α to assess the reference atoms for each volunteer.

Reference Atoms

To quantify the similarity of the observed topographies, we calculated the ccs between the reference atom and the 40 atoms building it plus the 10 atoms obtained from 10 virtual stimulation periods (cf. Section 2.3). The topography of a reference atom at maximum GFP is illustrated in Figure 4. The topographies vary over time (Section 2.3).

For the 40 + 10 stimuli, we observed a constantly high correlation from stimulus 10 to 43 in the correlation sequences. Before stimulus 10, we noted an upward trend for the ccs. For the correlations from the 10th stimulus to the 40th stimulus, coefficients were >0.9 for 7 out of 10 volunteers (Fig. 5). The correlation values for the 10 atoms calculated after the end of the real stimulation continued on the same level (cc >0.9) for 3 atoms and dropped thereafter to values comparable with the ones from the beginning of stimulation (Fig. 5).

Thus, a correlation sequence plateau (note that there are only 40 stimuli; the next 10 atoms describe the ongoing EEG/MEG after the end of stimulation) formed. For 3 out of 10 cases, we found a peak at stimulus 5, similar to the peak depicted in Figure 5. In 3 cases, we could observe that the EEG topographies became stable 4–6 stimuli later than the MEG topographies.

Furthermore, we went back to the averaged EEG/MEG data and noted that also the magnitude of the GFP increased over the first 7 to 10 stimuli. In addition, we checked the atoms calculated over the 40 + 10 stimuli and found a steady increase of the modulation parameter ξ in the stimulus range from 1 to 5 or 1 to 10 (depending on the volunteer) and a sudden decrease after stimulus 42/43. After 5 to 10 stimuli, the frequency of the atoms was equal to the individual α frequency. This effect occurred in both the EEG and MEG and could be observed only for volunteers only who showed α entrainment.

Some channels showed low correlation values, while most showed similarly high correlation values. Correlation sequences with a mean outside the 90% confidence interval with respect to the mean and SD of all the channels were rejected for the analysis of the correlation sequence plateau (Section 2.3).

Similarity of Topographies Between Different Frequencies

The correlation analysis described in Section 2.4 is now applied to all frequencies and all volunteers. Again, correlation sequences outside a 90% confidence interval were excluded from further investigation. Close to the individual α frequency, we found qualitatively the 3 phases of the correlation sequences (increase up to the 10th stimulus, plateau, decrease starting from the 3rd virtual stimulus) similar to the results in 3.1 for 7 out of 10 volunteers.

Subsequently, we categorized the correlation sequences obtained from all stimulation frequencies into the categories good, moderate, and weak. A good correlation sequence contained a clear rise of ccs within the first 10 stimuli, a stable correlation sequence plateau and a clear decrease after the 43rd atom. For the moderately distinct correlation sequences, an increase over the first 10 stimuli and a decrease after the 43rd atom was also required. However, the correlation plateau could be interrupted at up to five stimuli. For weak resemblances, the three phases mentioned above were not clearly distinguishable. The results are given in Table 1.

Inside the stimulation frequency plateaus, we can find very good to moderate correlation sequences, which is not or rarely the case outside of it. For the stimulation frequencies of 0.9α and 1.10α,

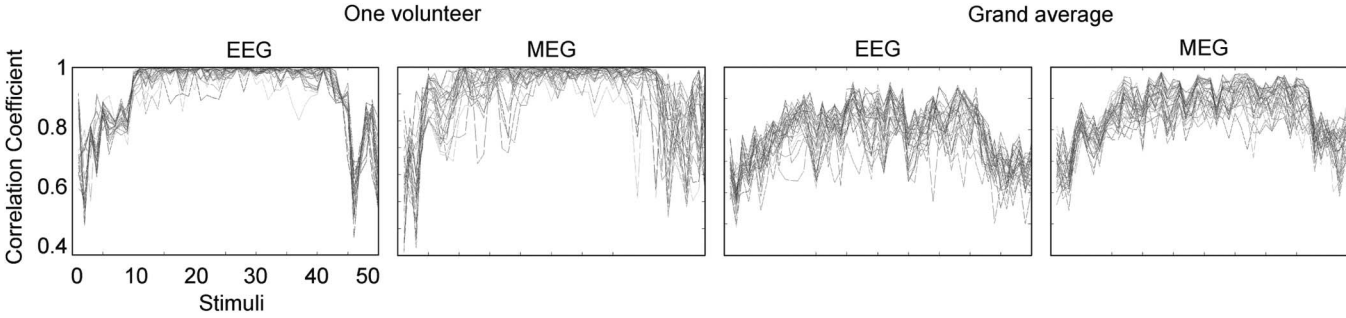

FIG. 5. Correlation coefficient sequences for all electroencephalogram channels and all magnetoencephalogram channels plotted over 40 + 10 virtual stimuli for stimulation at 1α (left: one volunteer; right: grand average for all volunteers). Note that the grand average included also those volunteers who did not show α entrainment. In all correlation sequences, we can see an increasing slope in the beginning and a decrease after index 43.

TABLE 1. Percentage of Subjects Who Show a Good, Moderate, or Weak Correlation Sequences

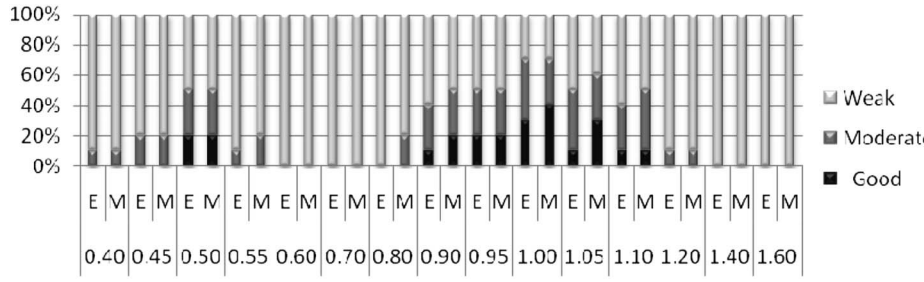

Good and moderate cases can almost exclusively be found in the close interval around the stimulation frequencies 0.5α and 1α.
E, electroencephalogram; M, magnetoencephalogram.

the number of very and moderately distinct correlation plateaus decreases. For 0.5α, we realized 2 very distinct and 3 moderately distinct correlation plateaus. The increase until the 10th stimulus and the decrease after the 43rd could still be verified statistically but was not as distinct as around 1α. This may be because of a lower signal-to-noise ratio resulting from weaker responses to stimulation. On the whole, we observed that we had slightly more good/moderate results for the MEG than for the EEG. According to the categorization (Table 1), the MEG scores equal or higher than the EEG.

For 3 out of 10 subjects, the increase took only 5 stimuli. However, the 3 subjects with an early increase at 0.5α are not the same as the 3 subjects who showed a peak at stimulus 5 at 1α. Figure 6 shows the grand average of the ccs for four different stimulation frequencies. Noticeable correlation plateaus were detected only inside the stimulation frequency plateau.

Setting a threshold at 0.75 for the correlation sequences revealed occipital and frontal regions of interest in the EEG. This was done separately for each subject and occurred only for stimulation frequencies within the plateau phase. When plotted onto a head surface, channels above the threshold form two continuous patches. In the occipital region, the energy in the observed channels was higher, in the frontal region lower. The MEG did show two distinct regions as well, showing similar energy content. The MEG is, however, located only over occipital part of the head.

This analysis was based on averaged data. The next section focuses on single-trial analysis.

Single-Trial Analysis

For 4 out of 10 volunteers, we obtained similar results to those described in the multitrial analysis in Section 3.2. Figure 7 displays the similarity between the individual reference and the single-trial atoms at 1α for 1 of the 4 volunteers. For approximately 10 stimuli, the ccs increased, thereafter the plateau was reached. For 2 to 3 periods after the end of the stimulation, we still found high ccs. Thereafter, the values dropped to the beginning values. We found this effect in EEG and MEG.

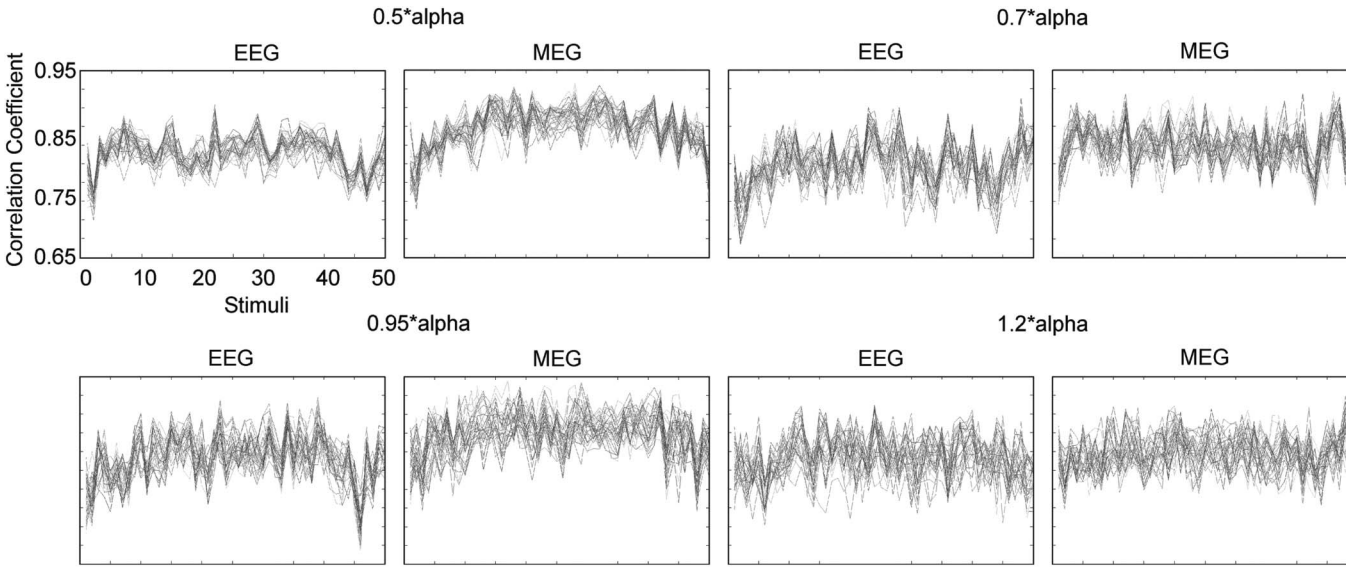

FIG. 6. Correlation values for all electroencephalogram channels and all magnetoencephalogram channels plotted over 40 + 10 virtual stimuli for stimulation at 0.5α, 0.7α, 0.95α, and 1.2α (grand average for all volunteers). Note that the grand average included also those who did not show α entrainment.

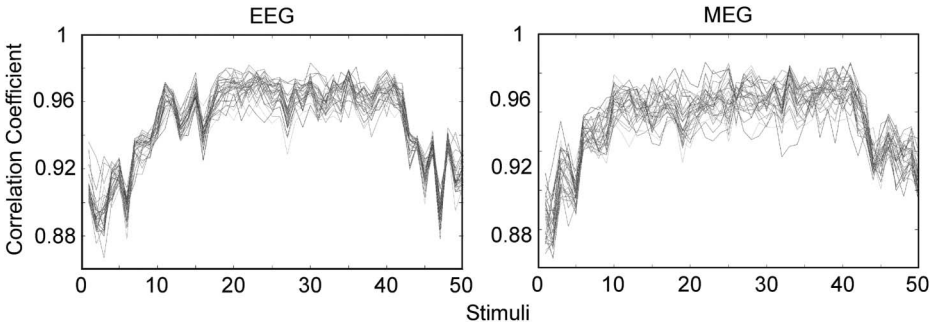

FIG. 7. Correlation values for all electroencephalogram channels and all magnetoencephalogram channels plotted over 40 + 10 virtual stimuli for stimulation at 1α for 1 volunteer (average over 20 single trains).

The results for the same volunteer at 0.5 and 0.7α are shown in Figure 8. As expected, we find for 0.5α the same qualitative behavior of the ccs as for 1α. This behavior is, however, not as pronounced. For 0.7α, this behavior cannot be found. Additionally, both the EEG and MEG channels show a more diverging behavior for 0.7α.

Furthermore, for the 4 out of 10 subjects who showed single-trial α entrainment, we calculated the variance of phase and frequency atom parameters across 20 trains for a series of stimuli (1 until 40 + 10). The variance was significantly elevated (i.e., was outside of the 90% confidence interval of the variance series computed for stimuli 11 until 40) for several stimuli after the start and after the end of stimulation for stimulation frequencies 0.95α until 1.05α. More precisely, the (consecutive) stimuli 1 until 6/7 and stimuli 43/44 and following were outside the confidence interval, while there were at most 3 violations of the confidence interval for stimuli 11 until 40. For other stimulation frequencies, only a varying number (1–6) of sporadic nonconsecutive outliers was found.

DISCUSSION

To our knowledge, in this article, for the first time intra-individually similar topographies at stimulation frequencies in an interval close to the individual α frequency and half of the α frequency are reported. We observed response plateaus in these intervals for both multitrial and single-trial data. An engaging/disengaging effect in the topographic analysis in both plateaus was discovered. The engagement effect is indicated by the increase of the ccs over the stimuli 1–10, which is accompanied by an adjustment of the frequency parameter calculated for atoms in the same stimulus interval and stimulation frequency. After the end of the stimulation, thus at atom 42/43 the disengagement effect occurs, which becomes apparent in the decrease of the ccs and the sudden adjustment of the frequency of the atoms. For stimulation frequencies outside the stimulation plateau neither did the observed topographies show similarity to the reference nor did the cc sequences show the engaging/disengaging effect.

In a first step, we calculated the cc sequences between the reference atom and the 40 atoms building it and 10 atoms calculated after the end of the real stimulation. We found that the correlation sequences can be divided into three phases: an increase, a correlation plateau, and a decrease. The latter started three stimulation intervals after the end of stimulation. We conclude that the visual system needs 5 to 10 stimuli to produce topographically stable responses that remain stable for 3 virtual stimuli after stimulation end. Furthermore, we can state that individually calculated reference atoms can indeed be used as reference in all volunteers.

In the multitrial analysis, we found that the cc sequences had qualitatively the same structure around 0.5α and 1α as had the cc sequences described for the reference atoms. In both cases, this occurred for 7 out 10 volunteers, which is in accordance to figures for α entrainment from literature (Lazarev et al., 2001).

For a stimulation frequency of 0.5α, we found a (dominant) response frequency coinciding with 1α. This response may be caused by phase/mode locking between the neural oscillator and the driving stimulation. Phase locking occurs if the fraction of the driving frequency and the natural frequency of the (driven) oscillator is rational. Out of the set of all stimulation frequencies, only 0.4α, 0.5α, 0.8α, 1α, and 1.6α can reveal rational fractions between the natural neural oscillator and the driving frequency. The rational fraction for 0.4α, 0.8α, and 1.6α however, respectively, coincide with the first, third and seventh harmonics of the natural frequency of the neural oscillator, thus—if detectable at all—are suppressed by the applied filter. The 0.5α (and of course 1α) has the first rational fraction at the fundamental frequency of the neural oscillator. Hence, stimulation with square waves at 0.5α may mainly elicit a response

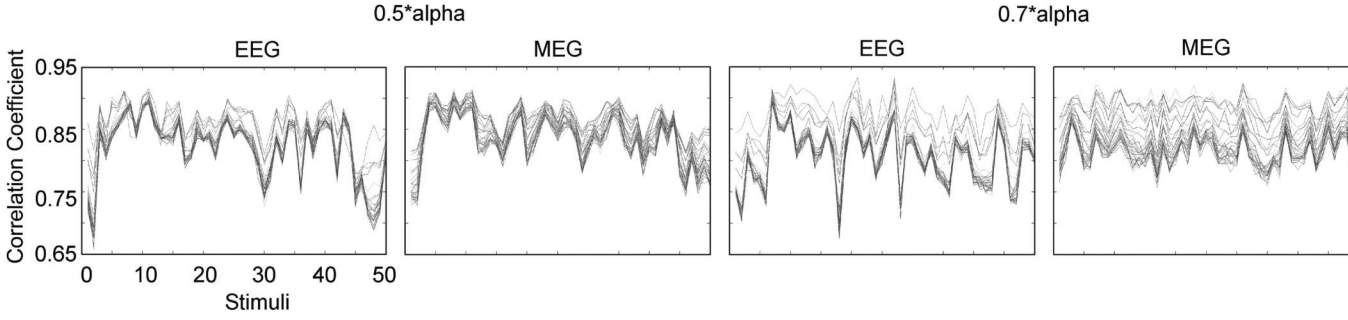

FIG. 8. Correlation values for all electroencephalogram channels and all magnetoencephalogram channels plotted over 40 + 10 virtual stimuli for stimulation at 0.5α (left) and 0.7α (right) for one volunteer (average over 20 single trains).

at the first harmonic of 0.5α because this coincides with the natural frequencies of the (nonlinear) neural oscillator.

The results for the single-trial analysis were not as distinct as for the multitrial analysis. We found analogous correlation sequences around 0.5α and 1α but only for 4 out of 10 volunteers. These four subjects were the same that showed the best results in multitrial analysis, which leads to the assumption that the signal-to-noise ratio was not sufficient in the other cases.

We chose to construct the reference atom from stimuli 1 to 40 instead of 10 to 40, because all 40 atoms represent the response to the complete stimulation sequence. Additionally, this allowed for a better comparability between the correlation sequence of the reference atom with the 40 atoms building it on one hand and the correlation sequences described above in multi and single-trial analyses on the other hand. We also performed a multitrial analysis for 3 volunteers were we used a reference atom built from stimuli 10 to 40 and noted no difference. Our explanation is that, because the magnitude of the GFP increases over the first 7 to 10 stimuli, the energy contained in atoms from the early stimuli is comparatively low, resulting in reduced influence on the average of the 40 atoms building the reference.

We interpreted the initial increase in the correlation sequences as an engaging effect of the assumed underlying network of oscillators. This view is supported by the fact that also the amplitudes in the averaged data increase with the first stimulation; furthermore, in the multitrial case, it takes approximately 10 stimuli to stabilize the responses and about 3 periods to destabilize after stimulation end. For any stimulation frequency outside the plateau phases, no such behavior was observed. In line with our interpretation, Fedotchev et al. (1990) noted during their photic driving experiments resonance phenomena when they changed the rate of stimulation frequencies from 1 to 15 Hz in steps of 0.05 Hz. However, for steps of 2 Hz, they observed weaker resonance peaks, which we understand as the consequence of insufficient stimuli of one frequency for a strong resonance to buildup.

The analysis of the phase and frequency parameters of the single-trial atoms computed for the 4 out of 10 subjects who showed an entrainment effect reveals more about the engagement process. We found significantly elevated values for variance of the phase and frequency parameters for stimuli 1 until 6/7 and 43/44 onward. The variance is bigger because of both increased and decreased values of the phase and frequency parameters. Phase parameters beginning on a level outside the confidence interval jump in an irregular fashion until they reach a stable/fluctuating state, which usually occurs after said six or seven stimuli. A change of the phase parameter can be translated to a neural oscillator, which is temporally accelerated/decelerated so that a higher/lower response frequency is determined. We interpret this behavior as shifting of the resting α activity toward the driving input. Thus, there are two kinds of synchronization, the first occurring between resting α activity and driving input and the second taking place between the cells in the primary visual cortex (indicated by the gradual increase of amplitude).

Evidence was recently presented for linear behavior of the brain's steady-state responses (Zähle et al., 2010). However, in contrast to (Zähle et al., 2010), who looked at the resonance frequencies that represent a large-scale measure, our study investigated the temporal dynamics of the steady-state response. We assume that large-scale measures would show linear aspects while more fine-grained measures show nonlinear behavior.

The topographic engagement and disengagement effects could be observed in slightly more subjects for the MEG than for the EEG. Additionally, MEG topographies are categorized (Table 1) equally or better (i.e., more *good* topographies instead of *moderate* ones) in comparison with EEG topographies. This result is in line with that of Schwab et al. (2006) who stated that their results were more pronounced in the MEG than in the EEG for all the volunteers for the same kind of stimulation. Thus, a more tangential than radial orientation of the underlying oscillator(s) could be assumed.

When we introduced a threshold for the correlation sequences, occipital and frontal regions of interest were found in the EEG. These regions were pronounced for stimulation frequencies within the plateau phase and contained higher energy in the occipital patch and lower energy in the frontal region. Based on the topography of the reference atom (Fig. 4), we assume that the occipital patch with higher energy content is produced by two or more sources that are located occipitally and influence the frontal region. This would explain the high correlation between channels. The two regions found in the MEG do not contradict our assumption, because the lower energy channels in MEG are located at the margin in direction toward the neck. Note that the MEG channels only cover the back of the head.

We chose to use one atom only, because according to the paired *t*-test (see Section 2.4) except for five cases only the first atoms were significant. The first MP-atom always had the highest energy content, describing the strongest oscillation in the signal. In our case, the first atom described the major oscillation of one or more symmetric and synchronous sources caused by the rhythmic stimulation, which can also be seen in the power spectra (Schwab et al., 2006). Note that one atom can describe topographies, which may have two or more underlying sources. Based on the results from Kawaguchi et al. (1993), who state that interhemispheric phase difference decreases during photic driving especially when individual EEG frequencies coincide with stimulation frequencies, at least two oscillator sources may be considered. Furthermore, Gray et al. (1989) demonstrated that neurons located in spatially separate columns in the visual cortex can show synchronous oscillatory responses. A more detailed answer about the amount of oscillators, their location, and temporal behavior can be given after a successful source localization study.

The MP Algorithm is able to approximate the data sufficiently for our purposes. In regard to the single-trial analysis, we must note the limitation set by the signal-to-noise ratio in some cases.

CONCLUSIONS

Our results support the assumption of a nonlinear information processing in the human visual system which may be described by a coupled oscillator system and provide an analysis of the topographic engagement/disengagement process.

ACKNOWLEDGMENTS

This work was supported by the Deutsche Forschungsgemeinschaft (DFG grant Ha 2899/7/8-1 and Wi 1166/9-1) and the BMBF grant 03IP605 and 01GQ0703 (Bernstein group Jena).

REFERENCES

Başar E. *Brain Function and Oscillations: Volume I: Brain Oscillations. Principles and Approaches*. New York; Springer-Verlag, 1998.

de Tommaso M, Stramaglia S, Schoffelen JM, et al. Steady-state visual evoked potentials in the low frequency range in migraine: a study of habituation and variability phenomena. *Int J Psychophysiol* 2003;49:165–174.

Fedotchev AI, Bondar AT, Konovalov VF. Stability of resonance EEG reactions to flickering light in humans. *Int J Psychophysiol* 1990;9:189–193.

Gebber GL, Zhong S, Lewis C, Barman SM. Human brain alpha rhythm: nonlinear oscillation or filtered noise? *Brain Res* 1999;818:556–560.

Gratkowski M, Haueisen J, Arendt-Nielsen L, et al. Decomposition of biomedical signals in spatial and time-frequency modes. *Methods Inf Med* 2008;47: 26–37.

Gratkowski M, Haueisen J, Arendt-Nielsen L, Zanow F. Topographic matching pursuit of spatio-temporal bioelectromagnetic data. *Przeglad Elektrotechniczny* 2007;83:138–141.

Gray CM, Konig P, Engel AK, Singer W. Oscillatory responses in cat visual-cortex exhibit inter-columnar synchronization which reflects global stimulus properties. *Nature* 1989;338:334–337.

Herrmann CS. Human EEG responses to 1-100 Hz flicker: resonance phenomena in visual cortex and their potential correlation to cognitive phenomena. *Exp Brain Res* 2001;137:346–353.

Jin Y, Potkin SG, Sandman CA, Bunney WE. Topographic analysis of EEG photic driving in patients with schizophrenia following clozapine treatment. *Clin Electroencephalogr* 1998;29:73–78.

Jin Y, Potkin SG, Sandman CA, Bunney WE. Electroencephalographic photic driving in patients with schizophrenia and depression. *Biol Psychiatry* 1997;41:496–499.

Kalitzin S, Parra J, Velis DN, Lopes da Silva FH. Enhancement of phase clustering in the EEG/MEG gamma frequency band anticipates transitions to paroxysmal epileptiform activity in epileptic patients with known visual sensitivity. *IEEE Trans Biomed Eng* 2002;49:1279–1286.

Kawaguchi T, Jijiwa H, Watanabe S. The dynamics of phase relationships of alpha waves during photic driving. *Electroencephalogr Clin Neurophysiol* 1993;87: 88–96.

Lazarev VV, Infantosi AFC, Valencio-De-Campos D, deAzevedo LC. Topographic aspects of photic driving in the electroencephalogram of children and adolescents. *Braz J Med Biol Res* 2004;37:879–891.

Lazarev VV, Pontes A, Genofre MA, deAzevedo LC. EEG photic driving in neuropsychiatric diseases in children. *Int J Psychophysiol* 2006;61:317.

Lazarev VV, Simpson DM, Schubsky BM, Deazevedo LV. Photic driving in the electroencephalogram of children and adolescents: harmonic structure and relation to the resting state. *Braz J Med Biol Res* 2001;34:1573–1584.

Mallat SG, Zhang ZF. Matching pursuits with time-frequency dictionaries. *IEEE Trans Signal Process* 1993;41:3397–3415.

Miranda de Sa AM, Infantosi AF. Evaluating the entrainment of the alpha rhythm during stroboscopic flash stimulation by means of coherence analysis. *Med Eng Phys* 2005;27:167–173.

Parra J, Kalitzin SN, Iriarte J. Gamma-band phase clustering and photosensitivity: is there an underlying mechanism common to photosensitive epilepsy and visual perception? *Brain* 2003;126:1164–1172.

Rager G, Singer W. The response of cat visual cortex to flicker stimuli of variable frequency. *Eur J Neurol* 1998;10:1856–1877.

Schwab K, Ligges C, Jungmann T, et al. Alpha entrainment in human electroencephalogram and magnetoencephalogram recordings. *Neuroreport* 2006;17: 1829–1833.

Silberstein RB. Steady-state visually evoked potentials, brain resonances, and cognitive processes. In: Nunez PL, ed. *Neocortical Dynamics and Human EEG Rhythms*. Oxford: Oxford University Press, 1995:272–303.

Stam CJ, Pijn JP, Suffczynski P, Lopes da Silva FH. Dynamics of the human alpha rhythm: evidence for non-linearity? *Clin Neurophysiol* 1999;110:1801–1813.

Takahashi T, Kamata K, Tsukahara Y. High-amplitude photic driving response and occipital lobe epilepsy. *Recent Adv Hum Neurophysiol* 1998;1162:565–569.

Zähle T, Lenz D, Ohl FW, Herrmann CS. Resonance phenomena in the human auditory cortex: individual resonance frequencies of the cerebral cortex determine electrophysiological responses. *Exp Brain Res* 2010;203:629–635.

